PROBING LUMINESCENCE FROM ASPHERICAL BUBBLE COLLAPSE

Claus-Dieter Ohl
Department of Applied Physics
TU Twente, Postbus 217
7500 AE Enschede
The Netherlands

Abstract

The luminescence from single laser produced cavitation bubbles for varying degrees of asphericity is investigated temporally, spatially, and spectrally resolved. The degree of asphericity is controlled with an adjustable rigid boundary nearby the bubble. Temporally, single and multiple light emission events happen during a time interval of 80 ns. The luminescence duration increases with increasing asphericity. Spatially, the emissions from aspherical collapsing bubbles display a pronounced halo around the central spot being several times larger than the luminescence from spherical collapse. Spectrally, the ratio of the line- to continuum emission of the sodium dublett is enhanced, whereas the total emitted energy decreases by four orders of magnitude as compared to the spherical collapse. These findings point towards emission not only from the bubble interior but also from the liquid surrounding the bubble exited by outgoing shock waves.

1 Introduction

The vast shrinkage of largely empty bubbles in a liquid, termed cavitation bubble collapse, is accompanied by the emission of shock waves and light. In the field of cavitation research the assumption of a spherical bubble shape for the entire life time helped to evaluate and interpret many experimental results: Even for largely deformed bubbles, having cylindrical, cigar and conical shapes, the volume dynamics has been successfully described with an effective bubble radius deduced from the occupied volume, see e.g. Godwin *et al.* (1999), Leighton (1999), and Versluis *et al.* (2000).

However, sphericity plays a crucial role at the last stage of bubble shrinkage, the moment of highest compression of the bubble interior and the liquid phase surrounding it. In the work of Ohl, Lindau and Lauterborn (1998) it was found that aspherical collapsing bubbles diminish or even cancel the light emission (SCBL, Single Cavitation Bubble Luminescence).

This paper presents a summary of experimental findings on the luminescence from cavitation bubbles where the spherical symmetry of the flow is disturbed in a controllable way. The cavitation bubbles are generated by focusing an intense (10-30 mJ) and short (8 ns FWHM) infrared light pulse from a Q-switched Nd:YAG laser tightly into a water filled cuvette. Cavitation bubbles produced this way differ from that in single bubble sonoluminescence (SBSL) experiments by size (0.6 mm to 1.9 mm maximum bubble radius) and by their life time. The much larger size offer clear advantages to study the collapse phase and the light emission, the time scales and spatial scales are resolvable with standard techniques such as with a fast photomultiplier and imaging with a microscope. Laser induced bubbles oscillate only a few times before they break up and dissolve. These *transient* bubbles grow out of the recombining hot plasma generated at the laser focus and become vapor bubbles similar to bubbles generated by boiling. They expand to a maximum size, and shrink afterwards. This shrinkage as it accelerates proceeds until it is stopped by energy dissipation mechanisms. These are mainly shock wave emissions into the liquid phase, localized heating of the bubble interior and viscous dissipation.

Two sources of asymmetry are present in the experiments: First the asymmetry introduced by the laser, because the focal region is rather cone like than spherical. Therefore, laser induced bubbles in their early stage aren't spherical either. However, during the growth, the bubble gains sphericity rapidly, and at maximum expansion deviations from a sphere could not be measured. When the bubble collapses, disturbances stored in the flow field are amplified and can severely influence the bubble shape at collapse. A quantification of this process is due to the nonlinearities involved a difficult task and will not be discussed in this paper. In general, the stability criterion given by Plesset and Mitchell (1956) is that during growth, $dR/dt > 0$, (R being the bubble radius) the surface is generally stable whereas during shrinkage surface modes are amplified. However, the growth rates of these modes depend on the amplitude of the initial disturbances. In the experiment this source of asymmetry is minimized by using a specially designed lens system which allows for a large focusing angle and thus a small, sphere like spot size, and by further limiting to small bubbles.

The second source of asymmetry are rigid and free boundaries nearby the bubble. In the experiments a rigid boundary at variable distance, s, is placed below or above the bubble. For large distances s of the boundary the undisturbed dynamics will be resolved. With decreasing distance s the boundary hinders the liquid in- and outflow, e.g. during the bubble collapse a jet flow towards the boundary is induced, see for example, Lauterborn and Bolle (1975). In the further text the results are presented using the normalized distance $\gamma = s/R_{max}$. For example, a bubble of normalized distance $\gamma = 1$ is at its maximum expansion a hemisphere.

Two different boundaries are used in the experiment: For the measurements of the temporal and spatial emission a rigid wall being large compared to the bubble radius, and for obtaining spectras the tip of a glass fiber which serves additionally as a light guide. In the absence of an additional boundary the γ-value is approx. 40, determined by the smallest achievable bubble of $R_{max} = 0.6$ mm and the focal distance of 25.4 mm to the nearest cuvette wall which is supporting the lens. Thus, in the text the term *spherical collapse* is used for a bubble collapse not influenced by additional boundaries.

2 Temporal Emission

The experimental setup to measure the duration and temporal shape of the luminescence event consists of a photomultiplier tube (Hamamatsu R5600U-3 with 650 ps rise time at a voltage supply of -800 V) connected to a digital sampling oscilloscope (TDS 784A, 1GHz analog bandwidth at a sampling rate of 4 gigasamples per second in single channel mode). The light emission from the bubble is imaged with a $f = 50$ mm lens onto the entrance window of the photomultiplier. The duration between bubble generation and collapse varies from shot to shot by a few percent, whereas the signal itself is a few orders of magnitudes shorter. To capture the luminescence signal at high sampling rates with the limited memory of the sampling oscilloscope, a delayed trigger mode is used. Here the light emission at time of bubble generation serves as the first/main trigger event, thereafter the oscilloscope after a delay time of $50\,\mu$s is rearmed and finally triggered by the cavitation luminescence.

The FWHM of the luminescence events is found to be as small as 4 ns which is in the range of the response time of the PMT, and of the reciprocal bandwidth of the input amplifier of the oscilloscope. Therefore, these recordings are compared to that from a impulse like signal. The light pulse from a frequency doubled Ti:Sapphire (395 nm) system with 200 femtosecond duration is fed into the same line measurement devices. The response of the system to the 200 fs laser pulse has a duration (FWHM) of 2.3 ns and exhibits that for low-pass filters typical overshoot following the signal. A Fourier deconvolution of the SCBL signal with the measured impulse response gives a difference in the luminescence duration of less than 10 %. Compared to the effort and introduction of further errors in the analysis no convolutions are done to the raw signals [1]. We conclude that the response of the measurement system is fast enough to capture the SCBL signal at high enough temporal precision.

The duration (FWHM) of the luminescence from *spherical* laser induced cavitation bubbles has already been measured by Ohl (1999), Ohl *et al.* (1999) and Baghadassarian *et al.* (1999) to be in the range of a few nanoseconds for bubble radii in the millimeter range. The luminescence duration increases linearly with

[1] Due to the sampling noise and the low, 6 1/2 bit effective sampling resolution frequency filtering during deconvolution is needed. The cut-off and the steepness of this filter are somehow arbitrary and introduce ambiguity.

increasing bubble radius. Before we will discuss in detail the dependencies on the pulse shape we first give general comments on the recorded signals:

- For unchanged experimental conditions the amplitude of the emission signal varies largely.
- The shape of the emission signal exhibits large variety. However, there is always a clear main maximum and up to three local maximums occur before, being denoted pre-cursors.
- The local maxima of the emission signal are distributed in a time interval of 80 ns around the main maximum. No emission is observed at other times, especially no emissions are found for the second collapse.
- The emission events are randomly distributed and can overlap. They might reach into the main maxima and become indistinguishable from it.

Now the structure of the light emission obtained with the photomultiplier is discussed. The time interval where emissions occur is around 40 ns before and after the main emission. Most of the emissions do happen before the main emission. This time interval is in the range where the acceleration of the bubble wall, $\ddot{R}$, changes sign: $\ddot{R} < 0$ to $\ddot{R} > 0$.

Further, the precursors are less pronounced for stronger luminescence events. An explanation for this might be, that the precursors originate from different *hot spots*. Either a strongly inhomogeneous bubble interior, or which might also be possible, a splitting of the bubble into parts. These parts might become compressed separately by the liquid inflow, by shock waves emitted from earlier collapsed splits or by a combined mechanism. A hint for this speculation is that larger bubbles exhibit stronger precursors. This bubbles are less spherical when they are produced and as discussed already stated more disturbed in the collapse phase.

By averaging the individual curves with their maximums superimposed, random events like the pre-cursurs are smeared. From these averaged pulses the pulse duration (FWHM) are determined. This type of averaging, being at first sight arbitrary, is similar to the method used in SBSL experiments, where averaging is done through autocorrelation over many emission events, see Gompf *et al.* 1997, or summing of streak photographs from multiple emission events, e.g. Pecha *et al.* (1998). This type of averaging would smear pre-cursors in SBSL, too.

2.1 Dependence on R_{max}

Figure 1 shows the luminescence signals, the inverted voltage of the PMT signal, for increasing bubble radii R_{max} from a) to f). This water-fall plots are composed from 100 individual runs, where the curves are sorted by amplitude and the position of the amplitude is shifted to $t = 0$. More than half of the curves exhibit a second and a few even a third local maximum. At first sight the time interval between the prepulses and the main maximum vary randomly. However, for curves with two maxima the mean interval, δt_{pm}, between the prepulse and the main maximum gives for $R_{max} = 0.64$ a $\delta t_{pm} = 12$ ns and increases to $\delta t_{pm} = 20$ ns for $R_{max} = 1.64$ mm. The amplitude for each set of experiment in Fig. 1 a) to f) varies by 400 %.

Figure 2 left compares the strongest signals for different R_{max}. For small bubble radii ($R_{max} = 0.64$ mm to $R_{max} = 1.09$) no second maxima is found and the pulse shape is nearly Gaussian. The larger bubbles possess a pre-cursor, which migrates into the main maximum for $R_{max} = 1.64$.

The averaged pulse shapes are given in Fig. 2 right. Here, the local maxima are smeared out without distorting the main pulse to much when compared with the individual signals in Fig. 2 left. The amplitude is increasing with increasing R_{max} up to $R = 1.45$ mm, for the largest bubbles the amplitude is less, $R_{max} =$ 1.64 mm.

The next figure 3 left summarizes the normalized energy, E, the pulse duration, τ and their intensities, $I = E/\tau$ of the averaged pulse shapes. The pulse duration (FWHM) τ increases with increasing maximum bubble radius from 4 ns to 9 ns.

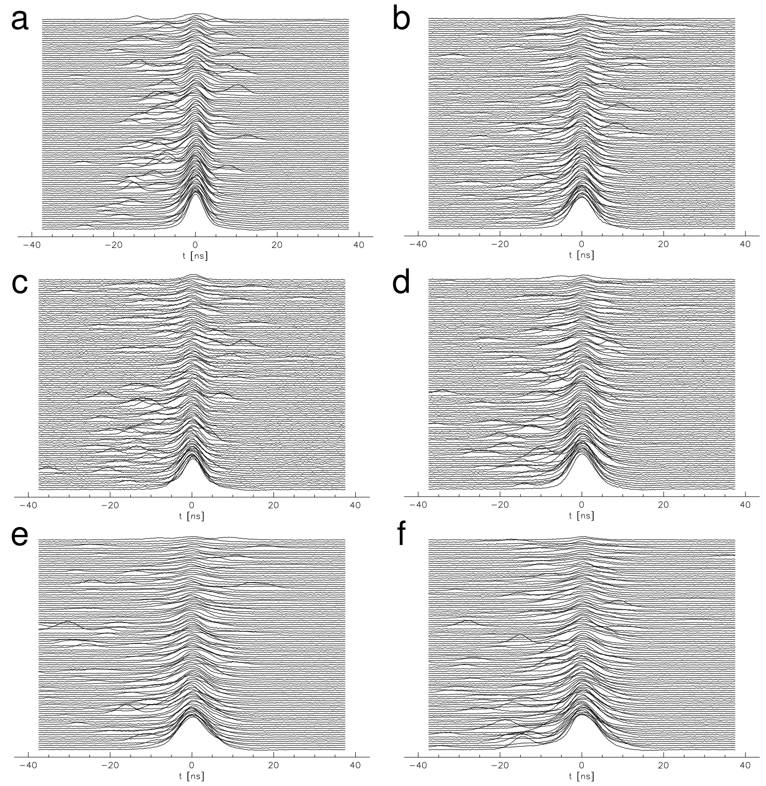

Figure 1: Waterfall plot of the inverted PMT signal for increasing $R_{\max}$ (a-i): The individual curves are sorted upwards with decreasing amplitude. The maximum of each curve has been shifted to $t = 0$. a) $R_{\max} = 0.64\,\mathrm{mm} \pm 0.09\,\mathrm{mm}$, b) $R_{\max} = 0.76\,\mathrm{mm} \pm 0.02\,\mathrm{mm}$, c) $R_{\max} = 0.88\,\mathrm{mm} \pm 0.05\,\mathrm{mm}$, d) $R_{\max} = 1.00\,\mathrm{mm} \pm 0.05\,\mathrm{mm}$, e) $R_{\max} = 1.09\,\mathrm{mm} \pm 0.03\,\mathrm{mm}$, f) $R_{\max} = 1.20\,\mathrm{mm} \pm 0.03\,\mathrm{mm}$.

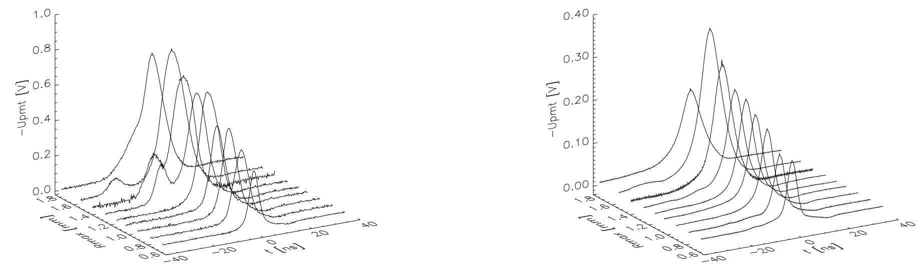

Figure 2: *Left:* Plot of the pulse shapes for the strongest photomultiplier signal from 100 luminescence events for different R_{max}. *Right:* Plot of the pulse shapes for the averaged photomultiplier signal from 100 luminescence events for different R_{max}

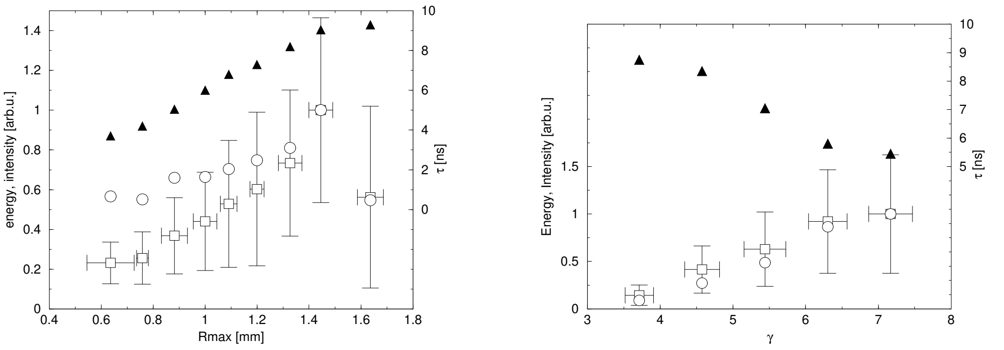

Figure 3: Plot of the emitted light energy (□), intensity (◯) and pulse duration τ (▲) in dependence on *left* the maximum radius and *right* in dependence on γ with a constant $R_{max} = 0.8\,\mathrm{mm}$. For a single data point 100 signals are superimposed. The error bars depict the standard deviation of the bubble radii and the amplitude of the individual signals, respectively. The light energy and the intensity are normalized respectively to their maximum values.

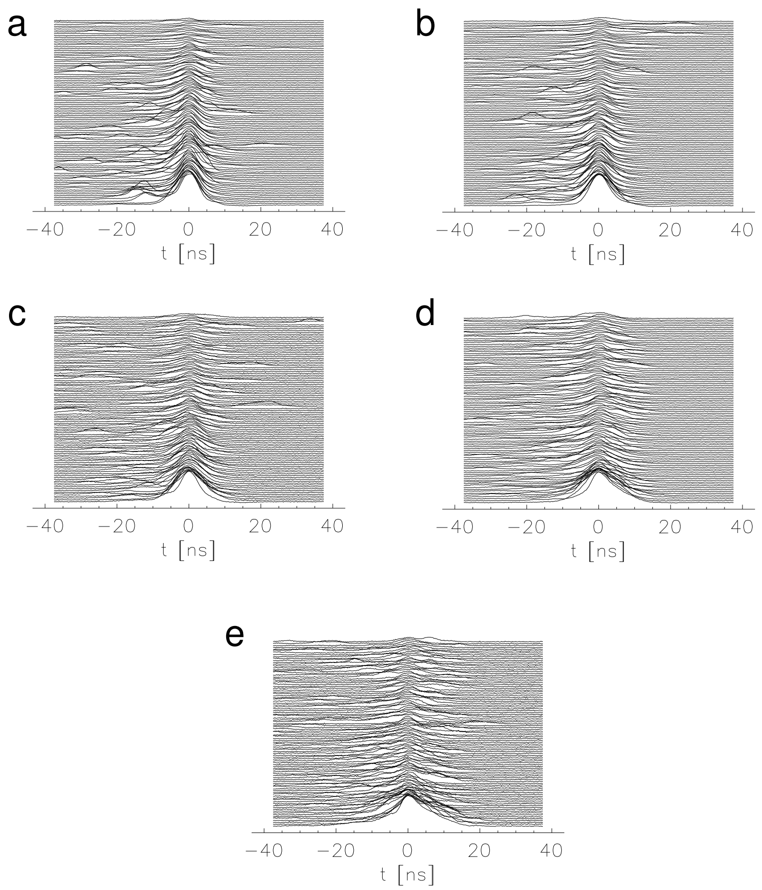

Figure 4: Waterfall plot of the SCBL emission for decreasing γ from a) to e): The individual curves are sorted upwards with decreasing amplitude. The maximum of each curve has been shifted to $t = 0$. $R_{\max} = 0.83\,\mathrm{mm}$ $\pm\, 0.06\,\mathrm{mm}$. a) $\gamma = 7.7 \pm 0.3$, b) $\gamma = 6.3 \pm 0.3$, c) $\gamma = 5.4 \pm 0.3$, d) $\gamma = 4.6 \pm 0.2$, e) $\gamma = 3.7 \pm 0.2$.

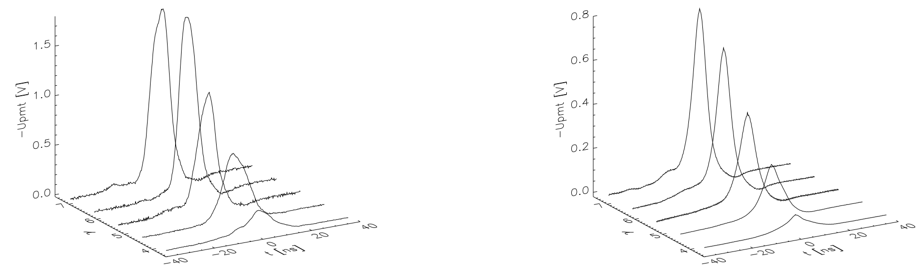

Figure 5: *Left:* Plot of the pulse shapes for the strongest photomultiplier signal from 100 luminescence events for different γ values. *Right:* Plot of the pulse shapes for the averaged photomultiplier signal from 100 luminescence events for different γ values.

2.2 Dependence on γ

We now focus on the dependency of the pulse shape on the stand-off parameter γ being varied between $7.7 \le \gamma \le 3.7$ for a constant maximum bubble radius $R_{max} = 0.8\,$mm. The water fall plots, Fig. 4, are given for five γ values decreasing from a) to e). Again we find multiple emission events during the collapse, with the strongest event occurring at last. With decreasing γ the amplitude of the prepulses decreases and the fall time of the main maximum increases significantly.

Again as for the spherical case, the strongest and the averaged pulse shapes are compared in Fig. 5 left. The amplitude decreases strongly for bubbles collapsing more closely to the boundary. Additionally, these shape becomes more angular as compared to the signals with no boundary present. These shapes can be explained with multiple emissions from different spatial positions. It seems, that for larger γ values, the two main emission events are responsible, however, with a more aspherical collapse $\gamma \le 4.6$, a qualitative change of the pulse is observed.

Averaging the signals, Fig. 5 right, pronounces these findings, for relative large γ values, the signal possesses a Gaussian shape whereas for smaller distances a triangular shape is found.

Figure 3 right collects the results of the pulse duration (FWHM), the emitted light energy and the intensity in dependency of γ from the averaged signals. The emitted energy increases by a factor of 5 from $\gamma = 3.7$ to $\gamma = 7.7$ and the pulse duration decreases from 8.8 ns to 5.5, which is about the value for the spherical case.

3 Spatial shape of the luminescence emission

In this chapter the spatial shape of a single luminescence event is investigated with means of gated photography. The imaging system consist of a long distance microscope (K2, Infinity), an image intensifier with a micro channel plate, MCP, (Proxity, PCO) and a CCD camera (KAF-1400, Kodak, having square pixel of $6.8\,\mu$ length). A relay lens maps the image from the phosphor screen of the images intensifier onto the CCD sensor. The image intensifier acts as fast shutter to suppress the strong plasma emission at time of bubble generation. Therefore, the microchannel plate is gated some time after the laser pulse around the expected time of bubble collapse. The gate is opened for $20\,\mu$ and afterwards the image is transfered to a lab computer.

The imaging system has a spatial resolution of $2.2 \times 2.2\mu\mathrm{m}^2$ per pixel for imaging the spherical collapse. However, for the aspherical collapse the emitted light decreases drastically. To account for the lower signal-to-noise ratios the CCD sensor was driven in binning mode, which adds the charges of four neighboring pixels. The binning mode increases the signal to noise ratio by a factor of 4 with the cost of a decrease in the spatial resolution decreasing to $4.4 \times 4.4\mu\mathrm{m}^2$ per pixel.

Examples of luminescence shapes are given in Fig. 6 for the spherical case and for an aspherical collapse with the boundary at a distance of 8 mm below ($\gamma = 10$) the central spot. These images are magnified gray scale pictures, the gray levels are rescaled linearly to the printable range. The line depicts the contour

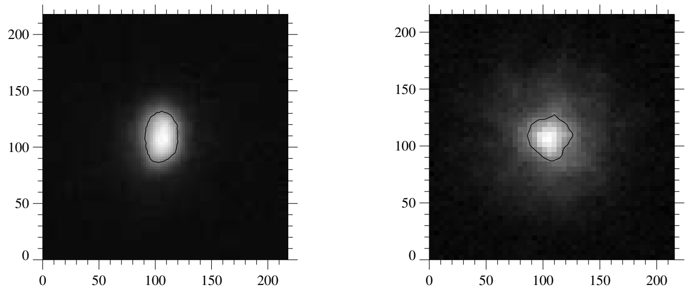

Figure 6: Typical photograph of the luminescence for a spherical collapsing (left) and with a boundary below collapsing bubble $\gamma = 10$ (right). The maximum bubble radius in both cases is $R_{max} = 0.8\,$mm. The scale is given in μm.

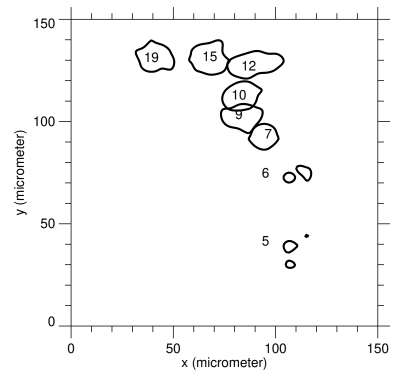

Figure 7: Position and shape of the averaged luminescence for different stand off parameters, printed besides the contour. The summing is done from the seven most brightest events from 100 laser generated bubbles. The maximum bubbles radius for all γ values is $R_{max} = 0.8\,$mm.

at 50% of the maximum pixel value. There are pronounced differences in the luminescence shape, and the structure exhibits some variablity. For a discussion on the luminescence shape averaged images have been generated. From 100 consecutive experiments the seven most brightest pictures are selected and averaged in two different ways. The events are added either with their position unchanged or by shifting them in such a way that their maximum overlay. The maximum bubble radius was kept constant to $R_{max} = 0.8\,$mm and the γ value varies from 19 to 5.

In Figure 7, where the images are superimposed without shifting, the contour of the central part of the luminescence structure is plotted for a range of γ values as indicated. With decreasing γ, the center of the luminescence moves downwards, and towards the right. The area enclosed in the contour decreases and for $\gamma = 6$ and $\gamma = 5$ it loses its integrity and consists of two, respectively three parts. We can account for the change in the vertical position: With a shorter distance to the boundary, the bubble is "attracted" stronger by the boundary, and therefore the collapse proceeds nearer to the boundary. The loose of integrity can be explained that the bubble splits and one or the other part is emitting most of the light. Thus through the summing, the brightest pixel belongs to changing parts of the divided bubble.

The change of the horizontal position can not be easily accounted for. It might be the combined attraction of the right cuvette wall, where the lenses for focusing the laser is built into in combination with the lower boundary. This would explain, why for smaller γ values where the lower boundary gains more influence, the change in the horizontal position is less.

In Figure 8 the same pictures for averaging of the luminescence are used but now they are superimposed at their brightest position. Therefore, we have a more specific look on the shape of the luminescence, independent on the variablity of the position of the luminescence. The emission for the spherical case ($\gamma = 31$) has an elliptical shaped area elongated normal to the boundary. This feature will be discussed

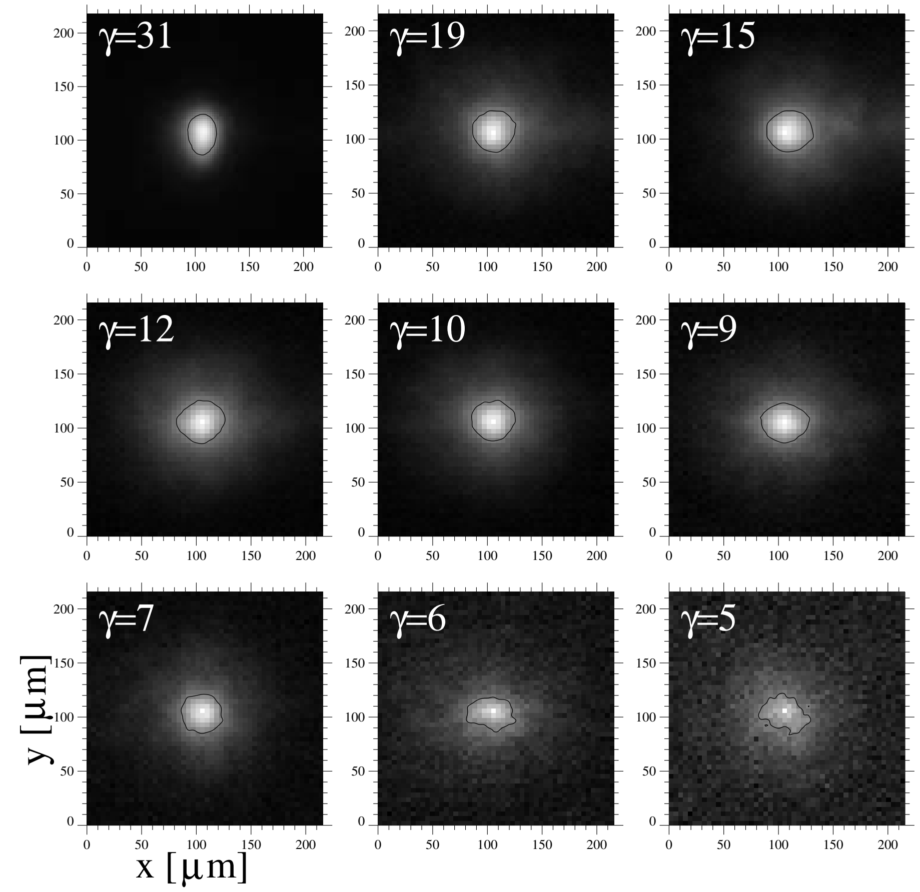

Figure 8: Luminescence averaged over 7 strongest emissions from one hundred events for decreasing stand off parameters.

later. The horizontal, D_h, and vertical, D_v diameters are $31\,\mu$m and $44\,\mu$, respectively. For the aspherical cases, the central part of the luminescence has a more circular shape, e.g. the diameters for $\gamma = 19$ are $D_h = 53\,\mu$m and $D_v = 57\,\mu$m. This size does not change much for smaller distances, however for the smallest distances,$\gamma = 6$ and $\gamma = 5$, with the very weak luminescence, it shrinks and due to the decreased signal to noise ratio, the contour becomes less smooth. An interesting feature in the aspherical cases is the "halo" around the central luminescing area. The extension of the halo, (taken at 10% of that of the maximum pixel value) is approximately $300\,\mu$m horizontally and $150\,\mu$m vertically for $\gamma = 19$, thus the area of the halo extends nearly fourteen times that of the central part. The size and structure of the halo is not changing much for different distances from the boundary. However, this halo has only been found in luminescence pictures with the boundary present. We can expect, that as the luminescence is much less localized in these cases, also the liquid is heated and part of the luminescence comes from excited water (OH^- emission). One candidate for the heating of the water is the emission of multiple shock waves. From high speed photography at 20 million and 100 million frames per second by, Ohl, Philipp and Lauterborn(1995) and Lindau and Lauterborn (2000), respectively, it has been observed that a shock wave is emitted when the liquid jet inside the bubble impacts onto the inward rushing opposing bubble wall. This impact transfers part of the liquid energy into acoustic energy. Therefore, less energy is available for heating of the bubble interior. Now we return to the spherical case: Individual and averaged pictures show an elliptical luminescence area elongated *normal* to direction of the laser beam. The bubble collapse proceeds elliptical, too, however it is rotated by 90 degrees! This difference is at first sight astonishing. It might be, that the surface mode of the elliptical bubble becomes unstable during collapse and changes its direction. However, slight changes in the laser energy which are always present would lead to different timing of this instability and we would expect different angles between the major axis of the luminescence spot and the laser beam. This has not been observed the individual pictures exhibit the same orientation of the major semi axis. Furthermore, in all photographic series of the bubble dynamics the major semi axis is aligned (as long as the bubble shape can be distinguished from the outgoing shock wave) parallel to the optical axis of the laser beam. A reproducible instability of the bubble shape at collapse leading to the observed luminescence shape can therefore be ruled out. A more convincing explanation is the following: Assuming a fixed aspect ratio of the semi axis throughout the bubble collapse and heating of the bubble interior by compression waves, the focal volume where light emission occurs will become aspherical either. The alignment of this heated volume relative to the bubble outline can be derived by a simple consideration. The compression waves from the equatorial parts of the bubble will be stronger as they travel over a longer distance compared to the polar ones. After reaching the center they will reflect into the less compressed part of the bubble. In spherical symmetry it was found numerically that most of the heating is done by outgoing reflected waves, see for example, Vuong *et al.* (1999). This consideration will hold also for the ellipsoidal case. Here the reflected and outgoing wave will evade into less compressed region, thus into the polar region. This mechanism of heating into the polar region has been investigated for SBSL type bubbles by Metten (2001) with molecular dynamics simulations.

4 Sodium Dublett Emission

In this last experimental section the modification of the emission spectra from aspherical collapsing bubbles is investigated. We concentrate on the sodium dublett emission from a 1 M (molar) aqueous solution of sodium chloride. No differences in the temporal emission between pure water and the emission in sodium chloride have been found, even for solutions with concentrations up to 3 M. The spectral properties of a single luminescence is to weak to become resolved. Therefore, many emissions have to integrated to resolve the spectrum and caution has to be taken to prevent recording from other light sources: Two conditions have to be fulfilled to obtain spectras with a satisfying signal to noise ratio: Short opening (gating) of the microchannel plate (MCP) at the time of luminescence and noiseless summing of the light emission onto the detector. The high contrast ratio of the MCP between its closed and its opened (gated) mode has been checked to suppress sufficiently the intense continuum emission from the dielectric breakdown at bubble generation. A Cerny-Turner type monochromator (ARC SpektraPro-275) with a 1200 lines/mm reflection grating blazed at 600 nm diffracts the light. The entrance slit was adjusted to 300 μm which allowed to resolved the dublett and still collects enough light. The exit slit of the monochromator has been replaced with the photocathode of the image intensifier. It's phosphor screen is imaged with a relay lens onto the CCD sensor. The triggering of the MCP is done in such a way, that the MCP is gated for a short time interval 20 μs during the expected SCBL emission.

For the summing over many SCBL emissions a low readout-noise and high resolution CCD (charge coupled device) was proven to be adequate (Quantronix, Photometrics, KAF 1440, 7 μm $\times$ 7 μm pixel size, cooled to -40 °C). The spectrometer was calibrated with the line emissions from a HeNe laser relative to it's internal calibration. A linear relationship was found between the position of the line on the CCD-sensor and the adjusted wavelength on the controller of the spectrometer. However, no radiance calibration was done, because only ratios of the spectrum over a small wavelength interval of 10 nm are investigated.

To collect and transport the light from the bubble to the entrance window of the spectrometer a quartz glass fiber was used, having a 600 μm core-diameter and being supported with a x-y-z translation stage. The polished tip of the glass fiber collects the luminescence and additionally acts as a rigid boundary. Therefore, the glass fiber was placed from above slightly tilted to the vertical into the cuvette. In Fig. 9 (left bottom) the used distances of the glass fiber tip to the laser focus are depicted. After every experimental run, the tip of the glass fiber was inspected not to be damaged by the strong acoustic transients present at bubble generation and collapse. A damage would influencing the light collection efficiency. No damage was found down to the closest distances presented here, however, the tip was fractured for distances below $\gamma = 2$. For each spectrum the light from 3000 laser generated bubble was summed, at a repetition rate determined by the laser frequency of 1 Hz it took 50 minutes to obtain a single spectrum.

The influence of the glass fiber inducing an aspherical bubble collapse is demonstrated in Fig. 10. Here the integrated spectral emission over the wavelength interval from 585 nm to 595 nm in dependence on the

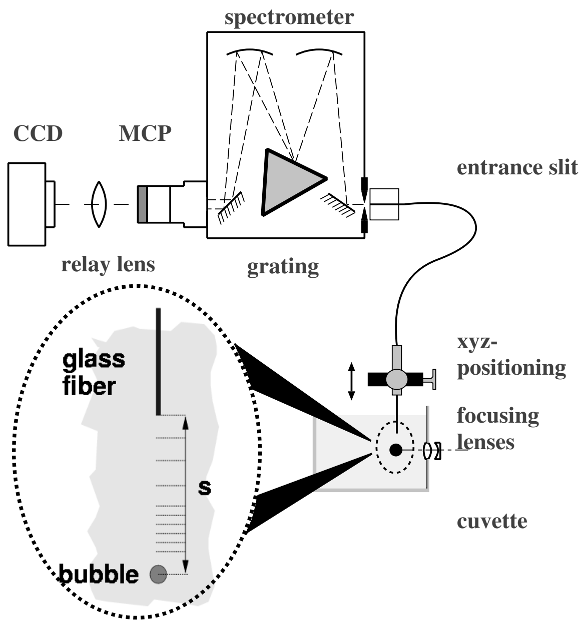

Figure 9: Experimental setup of the gated spectrometer together with a magnified view on the glass fiber. The different distances s between the bubble centers and the tip of the glass fiber are sketched in the magnified few.

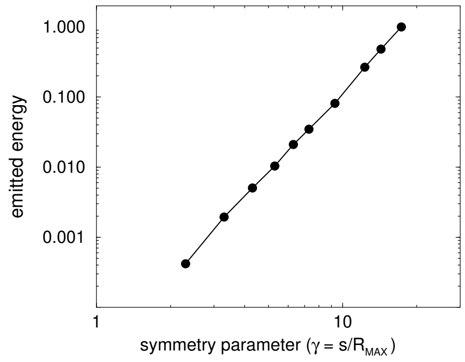

Figure 10: Influence of the distance on the emitted energy.

stand-off parameter γ is plotted. The intensity in Fig. 10 is corrected for the geometric light collection efficiency decreasing quadratically with increasing distance. The vertical axis covers more than 4 orders of magnitude.

Figure 11 shows the spectra for three different γ values. The two dashed vertical lines are depicting the position under spectral norm conditions at 589.0 nm and 589.6 nm. Within the resolution limit of the setup of 0.2 nm these lines are not shifted and no broadening can be found. Continuum emission is clearly visible. To evaluate the emission from the excited Sodium and that from sources leading to a contiuum emission, we define a ratio between the emission into lines and into the contiuum as indicated in Fig. 11 by the ratio of the areas A (enclosed by the curve and the x-axis) and B. Both areas start at 588.6 nm and end at 590.0 nm. The upper line of Box B is determined by the average of the emission in the wave length range from 585 nm to 595 nm. Thus the ratio A/B gives the relative emission energy (per wavelength) into the lines.

The varies ratios A/B obtained are plotted in Fig. 12. For increasing asphericity this ratio decreases first and than increases strongly. This finding hints to two different mechanisms leading to the sodium emission. Emission form the interior by heating of the sodium trapped in the bubble and emission from the liquid

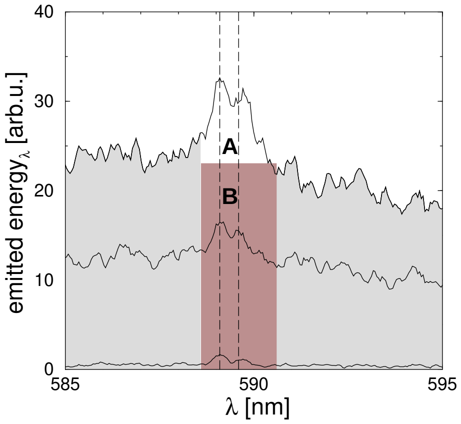

Figure 11: Spectra for different distances from top to bottom γ is 18.7, 13.3, and 4.7. The horizontal lines are at 589.0 nm and 589.6 nm. For the definition of A and B see the text.

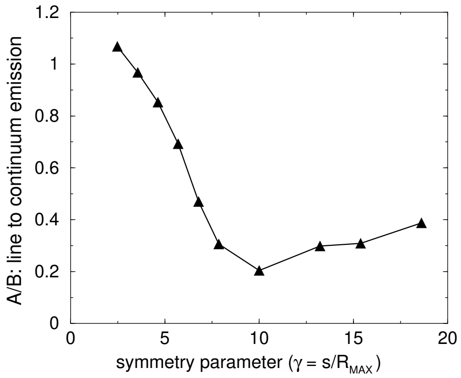

Figure 12: Ratio of line to continuum emission for different distances of the glass fiber from the bubble having a maximum radius of $R_{max} = 0.9\,\mathrm{mm}$.

surrounding the bubble. In the case for large γ values, the line emission comes mainly from the compressional heating of the sodium in the bubble and for the aspherical collapse (small γ values) the emission is excited mainly by shock waves from soluted sodium surrounding the bubble.

5 Conclusions

The amount of light emitted does depend very sensitive on the sphericity of the collapse. It has been shown that the emitted energy can be varied in a controllable way by 4 orders of magnitude. Photographs of the luminescing area revealed an increases of 14 times compared to that of a spherical collapse. There a localized ellipsoidal shape is found. This shape can be explained with heating by compression inside the bubble. The halo, observed from the aspherical bubble collapses might be the result of heating by a shock waves traveling in the liquid phase. These shock waves do not only origin from the bubble interior but can also be induced by the presence of the jet inside the bubble leading to a liquid-liquid impact. This explanation is supported by the spectral measurements. With increased asphericity, the line emission dominates the continuum emission as demonstrated for the sodium dublett emission. These findings point towards two important sources for light emission, one by compression waves inside the bubble and one from the heating by shock waves emitted into the liquid. The "large" laser induced cavitation bubbles have shown to be a valuable tool for investigating the physical mechanisms leading to luminescence.

Acknowledgments

The experimental work has been conducted at the Third Physical Institute at the University of Göttingen (Germany). There I have experienced numerous helpful hands and minds. From the many people I gratefully want to acknowledge I mention namely Prof. Dr. W. Lauterborn, Dr. T. Kurz and Dr. O. Lindau. The author is supported by the European Union under contract HPRN-CT-2000-00162.

References

Baghadassarian, O., Tabbert, B. and Williams G.A. (1999). Phys. Rev. Lett., **83**, 2437-2440.

Bourne, N.K. and Field, J.E. (1999). Phil. Trans. R. Soc. Lond., **A 357**, 295-311.

Crum, L.A. (1994). J. Acoust. Soc. Am., **95**, 559-562.

Godwin, R.P., Chapyak, E.J., Noack, J., Vogel, A. (1999). Los Alamos preprint LA-UR-99-0268.

Gompf, B. Gunther, R., Nick G., Pecha R. and Eisenmenger W. (1997). Phys. Rev. Lett., **79**, 1405-1408.

Lauterborn, W. and Bolle, H. (1975). *J. Fluid Mech.*, **72**, 391-399.

Leighton, T.G., Phelps, A.D., Cox, B.T. and Ho W.L. (1998). Acustica acta acustica, **84**, 1014-1024.

Lindau, O. and Lauterborn, W. (2000). AIP conference proceedings **524**, New York, 385-392.

Metten, B. (2001). Ph.D. thesis, 3. Physikalische Inst., University of Goettingen, Germany.

Ohl, C.D., Philipp, A. and Lauterborn, W. (1995). Annal. d. Physik, **4**, 26-34.

Ohl, C.D., Lindau, O. and Lauterborn, W. (1998). Phys. Rev. Lett., **80**, 393-396.

Ohl, C.D. (1999). Ph.D. thesis, Shaker Verlag Aachen, Germany, ISBN 3-8265-4556-7.

Ohl, C.D., Kurz, T., Geisler, T., Lindau, O., Lauterborn, W. (1999). Phil. Trans. R. Soc. Lond., **A 357**, 269-294.

Pecha, R., Gompf, B., Nick, G., Wang Z.Q. and Eisenmenger W. (1998). Phys. Rev. Lett., **81**, 717-720.

Plesset, M.S. and Mitchell, T.P. (1956). Quart. Appl. Math., **13**, 419-430.

Versluis, M., Schmitz, B., von der Heydt, A., Lohse, D. (2000). Science, **289**, 2114-2117.

Vuong, V.Q., Szeri, A.J. and Young, D.A. (1999). Phys. Fluids, **11**, 10-17.